Original research

Diagnostic accuracy of three-dimensional-rotational angiography and heavily T2-weighted volumetric magnetic resonance fusion imaging for the diagnosis of spinal arteriovenous shunts

Bikei Ryu [ID] ,[1,2,3] Shinsuke Sato [ID] ,[1,2,3] Masayuki Takase,[4] Tatsuki Mochizuki,[3] Shogo Shima,[3] Tatsuya Inoue,[3] Yoshikazu Okada,[3] Yasunari Niimi[1]

[1]Neuroendovascular Therapy, St. Luke's International Hospital, Chuo-ku, Tokyo, Japan
[2]Neurosurgery, Tokyo Women's Medical University, Shinjuku-ku, Tokyo, Japan
[3]Neurosurgery, St. Luke's International Hospital, Chuo-ku, Tokyo, Japan
[4]Radiology, St. Luke's International Hospital, Chuo-ku, Tokyo, Japan

Correspondence to
Dr Bikei Ryu, Neuroendovascular Therapy, St. Luke's International Hospital, Chuo-ku, Tokyo, Japan; ryu.bikei@twmu.ac.jp

ABSTRACT

Background Spinal arteriovenous shunts (SAVSs) are rare entities occurring in various areas, from the craniocervical junction to the sacral level. Recently, better understanding of SAVS angioarchitecture and elucidation of its pathogenesis have become possible with the advancement of imaging techniques. However, the utility of fusing different image modalities for SAVS diagnostics has not been determined. This study aimed to investigate whether three-dimensional-rotational angiography (3D-RA) and 3D-heavily T2-weighted volumetric MR (3D-MR) fusion imaging would improve the diagnostic accuracy for SAVSs.

Methods We retrospectively reviewed 12 SAVSs in 12 patients. Assessment of 3D-RA and 3D-RA/3D-MR fusion images for SAVS was performed by seven blinded reviewers. The final diagnosis was performed by two interventional neuroradiologists with extensive experience, and the interobserver agreement between the reviewers and the final diagnosis was calculated using κ statistics. The comparison of the interobserver agreement between 3D-RA and 3D-RA/3D-MR fusion images was performed for the diagnosis of SAVS subtypes. We also statistically compared the image-quality gradings (on a 4-grade scale) to delineate the 3D relationship between vascular malformations and the surrounding anatomical landmarks.

Results The interobserver agreement for the 3D-RA/3D-MR fusion images was substantial (κ=0.7071) and higher than that for the 3D-RA images (κ=0.3534). Significantly better image quality grades were assigned to 3D-RA/3D-MR fusion images than to 3D-RA images (p<0.0001) for the evaluation of the examined 3D relationships.

Conclusion The 3D-RA/3D-MR fusion images provided better interobserver agreement of SAVS subtype diagnosis, allowing for detailed evaluation of the SAVS anatomical structures surrounding the shunt.

INTRODUCTION

Spinal arteriovenous shunts (SAVSs) are rare entities arising in various areas, from the craniocervical junction to the sacral level.[1] Given the rarity of the condition, few studies have attempted to elucidate its pathogenesis. Therefore, factors related to the experience of the surgeons and neuroradiologists are likely to play a major role in the diagnosis and treatment strategy. Recently, with the advancement of imaging modalities and techniques, better understanding of SAVS angioarchitecture and elucidation of its pathogenesis have become possible.[2–6] In particular, three-dimensional-rotational angiography (3D-RA), including reconstruction with high spatial resolution of maximum intensity projection (MIP)-multiplanar reconstruction (MPR) images, has allowed investigators to better delineate the 3D relationship with the fine microvasculature and surrounding bony structures[2 5 7 8]; such images have been shown to provide a more exact depiction of anatomical details that are important in selecting the treatment strategy, resulting in increased treatment efficacy.[2 5–7] However, while 3D-RA has the advantage of being able to simultaneously visualize bony structures and blood vessels, it cannot visualize the surrounding soft tissues such as the spinal cord and surrounding dura mater.[2 9] The development of imaging methods that can depict both the neural structures and angioarchitecture would be valuable for the identification of the SAVSs in relation to the surrounding soft tissues, leading to diagnosis of the subtypes of SAVSs, which cannot always be easily discriminated.[5]

Recently, image fusion techniques between 3D-RA and high-resolution volumetric MRI have been widely used for diagnosis and pretreatment planning in the field of intracranial disease. Their utility to visualize the relationship between lesions and surrounding neuroanatomical structures has been reported,[10–13] but only a few studies have included SAVSs.[2 4 14 15] It is unknown whether fusion images are useful for the diagnosis of SAVS subtypes and evaluation of the precise angioarchitecture in coherent cases of SAVSs and, to our knowledge, no comparative analysis with fusion images has been reported. The purpose of this study was to determine the technical feasibility of creating 3D-RA and high-resolution volumetric spinal MR fusion images. Furthermore, we compared their interobserver agreement for precise subtype diagnosis to that of 3D-RA alone, and the diagnostic accuracy of the fusion images to assess the anatomical characteristics of SAVSs was evaluated.

METHODS

All procedures performed in this series involving human participants were in accordance with the ethical standards of the institution and with the 1964 Helsinki declaration and its later amendments or comparable ethical standards. The requirement for written informed consent was waived because of the retrospective design. The STROBE guidelines were followed in this study.

Patients

This retrospective study included 41 consecutive patients diagnosed with SAVSs between January 2015 and December 2020. Of these, the data of 12 patients were analyzed for whom both preoperative 3D-heavily T2-weighted volumetric MRI (3D-MRI) and conventional digital subtraction angiography (DSA) with 3D-RA data were available. Demographic data, baseline clinical status, and imaging results were also collected from the medical records. 3D-RA/3D-MR fusion images were created for these 12 patients.

The diagnosis and detailed angioarchitecture of the SAVSs were evaluated based on multimodal imaging including 3D-RA/3D-MR fusion images. SAVSs were further classified based on previous studies according to the shunt location: spinal cord arteriovenous malformation (SAVM), perimedullary arteriovenous fistula (PMAVF), spinal dural AVF (SDAVF), spinal epidural AVF (SEDAVF), and radicular AVF (RAVF).[2 5 6]

Imaging

A biplane angiography system (Artis zee Q, Siemens Healthcare GmbH, Forchheim, Germany) was used for conventional spinal DSA. All patients underwent spinal angiography under general anesthesia. In addition to conventional DSA, 3D-RA of the main feeding artery was subsequently performed using a 30×40 cm flat panel detector. The parameters were: resolution of 960×960 pixels (30×30 cm), image acquisition covering 100°, left anterior oblique to 100° right anterior oblique in a screw axis rotation of the C-arm with the X-ray tube moving under the patient, total acquisition time of 5–20 s for 133 projection images, 70 Kv using the 360 nGy/frame dose mode, and angulation step of 1.50°/frame.

The MIP and volume rendering (VR) technique were also used for the 3D display. The obtained fusion 3D data were reconstructed into thin 1.0–5.0 mm slab-MIP images. Conventional spinal DSA and reconstructed images obtained from 3D-RA with adjustable transparency of the surrounding structures were used to analyze the detailed angioarchitecture and anatomical relationships of the SAVSs.

Preoperative 3D-heavily T2-weighted volumetric spinal MRI was performed using a 3.0 Tesla imaging system (CUBE: Discovery MR750w, GE Healthcare, Milwaukee, Wisconsin, USA and VISTA: Phillips Medical Systems, Eindhoven, The Netherlands). The T2 sagittal CUBE parameters (fast spin echo 3D) were: slice thickness, 1.6 mm; ACQ voxel size, $0.75 \times 0.83 \times 1.6$ mm (freq×phase×thickness); REC voxel size, $0.47 \times 0.47 \times 0.8$ mm (freq×phase×thickness); freq field of view (FOV), 24; phase FOV, 0.7; repetition/echo time, 1500/90 ms; scan time, 5 min 10 s. A 26-channel body 36 AA coil was used. The T2-coronal VISTA parameters (fast spin echo 3D) were: slice thickness, 0.8 mm; ACQ voxel size, $0.87 \times 0.91 \times 0.8$ mm (freq×phase×thickness); REC voxel size, $0.49 \times 0.49 \times 0.8$ mm (freq×phase×thickness); FOV, 250 mm; RFOV, 100%; repetition/echo time, 1500/109 ms; scan time, 5 min 36 s. A 28-channel coil (dS torso coil [16 ch] + posterior coil [12 ch]) was used.

3D-RA/3D-MR fusion image processing and data analysis

Commercially available experimental reconstruction software (Syngo X workplace VD20B, Siemens) was used for the reconstruction and fusion of the 3D-RA and 3D-MRI data in a 3D workstation (XLeonardo with Dyna3D, Siemens Medical Solutions). The fusion of both imaging modalities was performed semi-automatically. After the automatic co-registration, manual co-registration was performed to reach the optimal overlap of the anatomical structures, including the vertebral bone and T2 flow voids, by experienced neuroradiology technologists with the assistance of neurointerventionalists. The obtained 3D data were reconstructed into 1.0–5.0 mm thin slab-MIP images and MPR images. The contrast window level was separately adjusted to achieve correct visualization. Appropriate quality fusion images could be created in approximately 15 min.

We retrospectively examined the images obtained from all patients, and the obtained images were simultaneously evaluated by two well experienced interventional neuroradiologists (consulting specialists, board certified members of the Japanese Society of Neuroendovascular Therapy (JSNET) with over 40 and 20 years of clinical experience, respectively). The angioarchitecture, including shunt location, feeders, and drainers, in relation to the surrounding anatomical structures was analyzed in detail. At the end of each case review the two consulting specialists made the final diagnosis of the SAVSs as a reference standard.

For the purpose of assessing the diagnostic accuracy of each reconstructed image, seven blinded reviewers (two specialists of the JSNET with 20 and 12 years of clinical experience, respectively, and five neurosurgery fellows) independently diagnosed the subtype of SAVSs, including the shunt point, and scored the quality of the obtained 3D images in all cases. In this study, two review sessions were performed for the diagnostic accuracy of the SAVSs. The reviewers assigned these ratings in two steps. In the first session the reviewers independently evaluated the angioarchitecture of each case with 3D-RA without using 3D-RA/3D-MR fusion images. In the second session the reviewers evaluated the angioarchitecture with the addition of the 3D-RA/3D-MR fusion images and scored the image quality of each case again. Both sessions were performed independently, and each review session included SAVSs subtype diagnosis, diagnosis of the shunt point, and evaluation of the quality of the images. A 4-grade scale (1=Poor, 2=Moderate, 3=Good, 4=Excellent) was used to score the image quality to elucidate the relationship between the vessels and surrounding anatomical structures including the spinal cord, dura mater, subarachnoid space, and bone and soft tissues. Based on the review results, we statistically analyzed whether the 3D-RA/3D-MR fusion images contributed to the diagnosis of the SAVS subtypes and to the delineation of their anatomy.

Statistical analysis

The final diagnoses and shunt points of the SAVSs judged by the two consulting specialists were compared with the answers of the seven blinded reviewers. We statistically analyzed the interobserver agreement using the κ statistic (Fleiss' κ value) between the seven blinded reviewers' results and the final diagnosis of each case produced by the consulting specialists, and the interobserver agreement was determined by calculating the κ coefficient: κ<0, poor; κ<0–0.20, slight; κ=0.21–0.40, fair; κ=0.41–0.60, moderate; κ=0.61–0.80, substantial; κ=0.81–1.00, almost perfect agreement.[16] The comparison of the accuracy of the shunt points and the image quality assessed on the 4-grade scale with and without the use of the 3D-RA/3D-MR fusion images
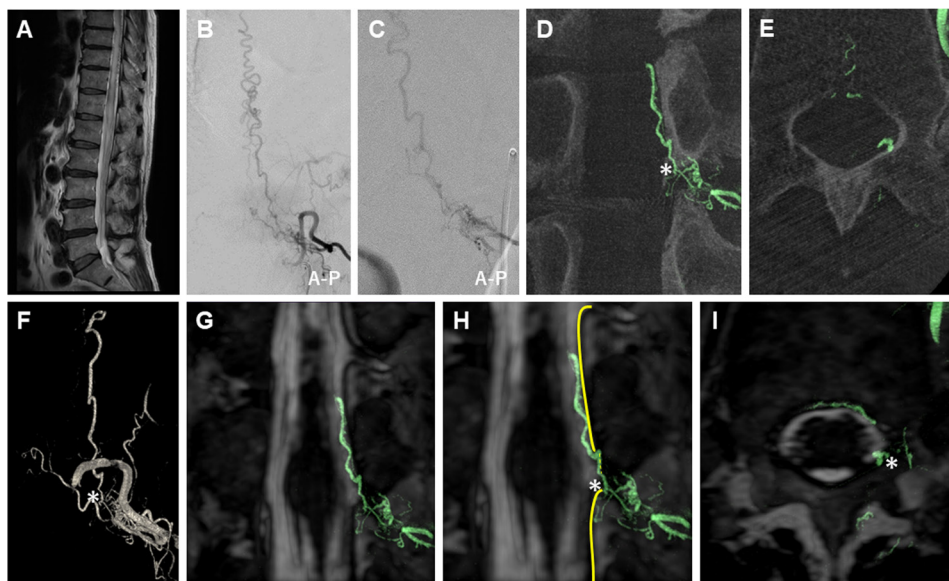
Figure 1 3D-RA/3D-MR fusion images of a SDAVF (case 1). Preoperative clinical imaging of a SDAVF in a patient in their 70s who presented with progressive myelopathy. Thoracolumbar sagittal T2-weighted MRI (A) shows high intensity of the spinal cord and dilated tortuous vessels around the spinal cord. Selective left Th12 segmental artery angiography (B) and selective microcatheter angiography of the feeding artery (C) show an arteriovenous fistula with a single drainage vein into the radiculomedullary vein supplied by multiple fine feeders from the radiculomeningeal artery. MIP coronal (D), axial (E), and volume rendering (F) images reconstructed from the 3D-RA of the left Th12 segmental artery show the detailed angioarchitecture of the SDAVF. 3D-RA/3D-MR fusion images (slab MIP coronal images (G, H) and axial image (I)) show the clear 3D relationship with differential contrast between the detailed angioarchitecture of the SDAVF and the surrounding tissue structure, suggesting that the SDAVF shunts into the radiculomedullary vein on the dura mater of the spinal nerve root sleeve (G–I). The dura mater is clearly visualized by a black line in contrast to the spinal fluid in the subarachnoid space. The asterisk indicates the shunt point. The yellow line indicates the dura mater of the spinal canal. 3D-MR, three-dimensional-heavily T2-weighted volumetric magnetic resonance; 3D-RA, three-dimensional-rotational angiography; A-P, anterior-posterior; MIP, maximum intensity projection; MRI, magnetic resonance imaging; SDAVF, spinal dural arteriovenous fistula.

was performed using Pearson's χ^2 test. The significance level was set at p<0.05. All statistical analyses were performed using JMP Pro15 (SAS Institute, Cary, North Carolina, USA).

RESULTS
Patient demographics and SAVS characteristics
The 12 included patients underwent conventional spinal DSA, 3D-RA, and 3D-MRI for evaluation of the SAVSs. 3D-RA was performed at the level of the noted lesion to better delineate the angioarchitecture. Fusion, VR, and reconstructed MPR-MIP images obtained from 3D-RA were also evaluated. Based on the final consensus diagnosis of the two consulting specialists, three patients had PMAVFs, three had SDAVFs, four had SEDAVFs, one had SAVM, and one had RAVF. The patient demographics and SAVS characteristics are summarized in online supplemental table 1.

Diagnostic accuracy of the 3D-RA/3D-MR fusion images of the SAVSs
The 3D-RA/3D-MR fusion images were successfully processed in all patients (see figures 1–3 and online supplemental figures 1–5). Fusion images provided easier recognition of the 3D spatial relationship between the angioarchitecture of the SAVS and surrounding tissues, including the spinal cord, dura mater, bony structures, and subarachnoid space. The image quality grade was significantly higher in the 3D-RA/3D-MR fusion images than in the 3D-RA images (3D-RA: poor 20.3%, moderate 46.4%, good 33.3%, excellent 0% vs 3D-RA/3D-MR fusion image: poor 1.2%, moderate 3.6%, good 36.9%, excellent 58.3%, p<0.0001, figure 4A). The detailed structure of the SAVSs, including the course of feeders/drainers, surrounding

structures, and their 3D relationship with high spatial resolution, could be clearly identified. The diagnostic accuracy of the SAVS subtypes was significantly higher in the 3D-RA/3D-MR fusion images than in the 3D-RA images (86.9% vs 59.5%, p<0.0001). There was no significant difference between the 3D-RA and 3D-RA/3D-MR fusion images in terms of the accuracy rate for identification of the shunt points (correct identification, 3D-RA 66.6% vs 3D-RA/3D-MR fusion image 76.1%, p=0.1719).

Interobserver agreement for the diagnosis of SAVSs with the 3D-RA/3D-MR fusion images
For all reviewers, the use of fusion images increased the concordance rate with the final diagnosis (figure 4B). Overall, interobserver agreement was fair for the diagnosis of SAVSs using 3D-RA with conventional DSA (κ=0.3534, figure 4B), but it was substantial when also using the 3D-RA/3D-MR fusion images, with a higher kappa coefficient (κ=0.7071, figure 4B). The interobserver agreement for the diagnosis with 3D-RA differed between specialists and fellows (κ=0.5514 vs κ=0.2751, figure 4A), but using the 3D-RA/3D-MR fusion images increased the interobserver agreement (κ=0.7778 vs κ=0.6494, figure 4B).

For each diagnostic category, the 3D-RA dataset alone did not provide sufficient interobserver agreement except for SAVM (SAVM: κ=0.7573, PMAVF: κ=0.4108, RAVF: κ=0.2208, SDAVF: κ=0.1418, SEDAVF: κ=0.3015, figure 4C). The 3D-RA/3D-MR fusion images improved the understanding of the anatomical relationships and increased the interobserver agreement for the diagnosis of the SAVS subtype (SAVM: κ=0.6862, PMAVF: κ=0.6281, RAVF: κ=0.8205, SDAVF: κ=0.6372, SEDAVF: κ=0.8036; see figure 4C and online supplemental figure 6).
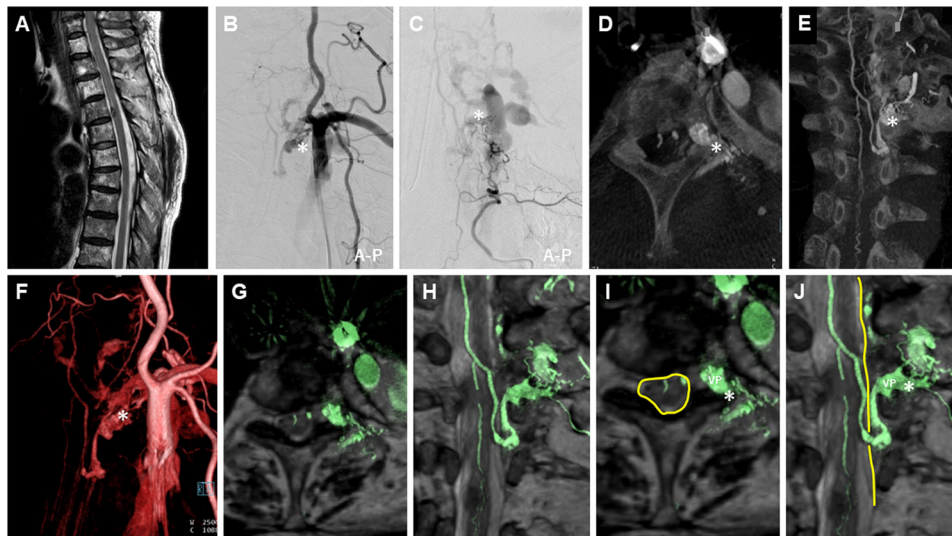
Figure 2 3D-RA/3D-MR fusion images of a SEDAVF (case 2). Preoperative clinical imaging of a SEDAVF in a patient in their 60s who presented with muscle weakness and sensory disturbance of the lower extremities. Thoracic sagittal T2-weighted MRI (A) shows low signal intensity of the ventral spinal cord at the Th4 level. Subclavian artery angiography (B) and selective left Th4 segmental artery angiography (C) show a SEDAVF with an epidural VP supplied by the left supreme intercostal artery and dorsal somatic branch. MIP axial (D), coronal (E), and volume rendering (F) images reconstructed from the 3D-RA of the left subclavian artery show the detailed angioarchitecture of the SEDAVF. The arteriovenous fistula drains into the intradural perimedullary vein through the epidural VP located in the lateral epidural space. 3D-RA/3D-MR fusion images (slab MIP axial image (G) and coronal image (H), slab MIP image with scheme (I, J)) show a clear 3D relationship with differential contrast between the detailed angioarchitecture of the SEDAVF and surrounding tissue structure, suggesting that the SEDAVF shunts into the lateral epidural VP. The dura mater is clearly visualized by a black line in contrast to the spinal fluid in the subarachnoid space. An epidural vein draining from the VP penetrates the dura mater of the spinal canal. The draining vein ascends the subarachnoid space and converges on the perimedullary vein. The asterisk indicates the shunt point. The yellow line indicates the dura mater of the spinal canal. 3D-MR, three-dimensional-heavily T2-weighted volumetric magnetic resonance; 3D-RA, three-dimensional-rotational angiography; A-P, anterior-posterior; MIP, maximum intensity projection; MRI, magnetic resonance imaging; SEDAVF, spinal epidural arteriovenous fistula; VP, venous pouch.

DISCUSSION

In this study we evaluated whether using 3D-RA/3D-MR fusion images would improve the diagnostic performance for SAVSs. The interobserver agreement for the diagnosis, expressed with the kappa coefficient, markedly improved using fusion images. In particular, the diagnostic accuracy of the fusion images in the evaluation performed by the fellows was remarkable, and acceptable agreement was noted between the fellows and the expert diagnoses. The fusion images allowed significantly better recognition of the spatial relationship between the angioarchitecture of the SAVSs and the surrounding anatomical landmarks, including bony and soft structures, than 3D-RA with conventional DSA alone. The results of the present study show that the addition of 3D-RA/3D-MR fusion images changed the diagnosis of the lesions, suggesting that only using conventional DSA with 3D-RA may lead to misdiagnosis. There was no significant difference between the 3D-RA and 3D-RA/3D-MR fusion images for the accurate identification of the shunt points. This finding indicates that 3D-RA with conventional DSA is valuable for the identification of shunt points. However, the categorical diagnosis of the SAVS subtype is determined based on the anatomical landmarks where the shunt occurs. Thus, fusion imaging may be essential for precise categorical shunt type diagnosis. To our knowledge, this is the first study to confirm the diagnostic accuracy of 3D-RA/3D-MR fusion images for the evaluation of SAVSs. Our fusion images provided a more detailed understanding of anatomy than 3D-RA without increasing the X-ray exposure of the patient. Unlike time-resolved imaging of contrast kinetics or computed tomography-myelography,[14 15] the 3D-MRI used in our fusion images can be obtained without the administration

of contrast or the need for lumbar puncture. The advanced 3D-RA-MR fusion technique enabled simultaneous visualization of the precise angioarchitecture of the SAVSs. 3D-RA/3D-MR fusion imaging is a promising technique to precisely visualize SAVSs, but further studies with larger samples are required to confirm the utility of this fusion technique.

The complex vasculature of SAVSs occasionally renders surgical and endovascular treatment challenging. It is difficult to delineate this complex vasculature with only conventional DSA because of its 2D acquisition and inherent vessel overlap. Thus, it is well known that 3D-RA provides accurate evaluation of the shunt angioarchitecture with high spatial resolution and more precisely shows the relationship between the shunt point and the surrounding bony structures than conventional DSA.[7 8] However, the spinal cord and surrounding soft tissues including the dura mater are poorly distinguishable and recognizable with 3D-RA. For this reason, some SAVSs are often misdiagnosed as another type of SAVS at individual centers or there are diagnostic disagreements even among experts.[2 5]

Recently, the T2-weighted volumetric spinal MR sequence was also shown to be well suited for the identification of vascular flow voids with a high degree of accuracy of detection, localization, and characterization of SAVSs.[17–20] Clear visualization of even subtle flow voids and neural structures could be achieved.[20] However, fine arterial feeders and draining veins cannot be visualized and the actual fistula point cannot be seen with this sequence alone. The type of spinal vascular malformation cannot be completely differentiated with MRI alone.[18 21] Conversely, this volumetric sequence provides high spatial resolution and tissue interface contrast between the parenchyma, cerebral
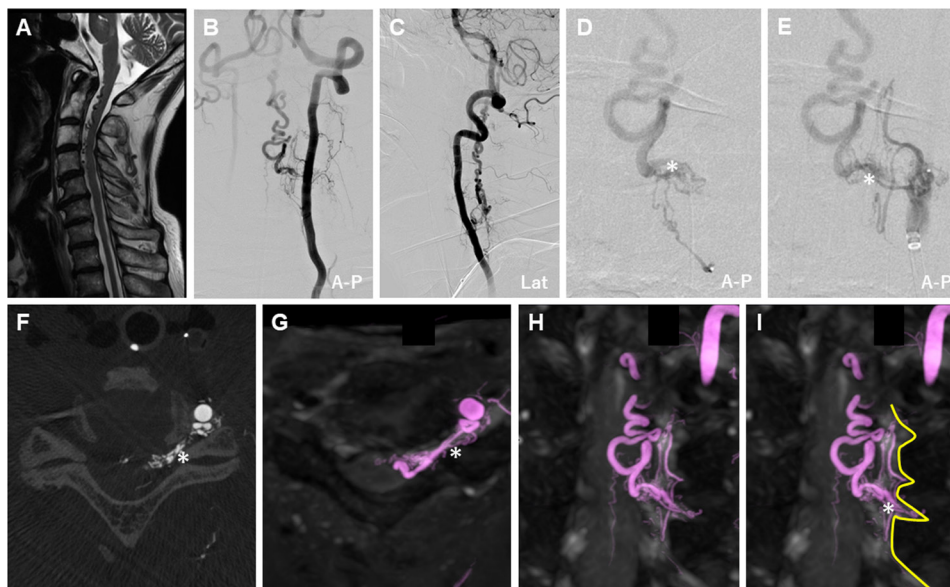
Figure 3 3D-RA/3D-MR fusion images of a RAVF (case 3). Preoperative clinical imaging of a RAVF in a patient in their 70s who presented with muscle weakness of the extremities. Cervical sagittal T2-weighted MRI (A) shows dilated tortuous vessels around the ventral cervical spinal cord. Left vertebral artery angiography (B, C), selective left C6 segmental artery angiography (D), and selective left C5 segmental artery angiography (E) show the spinal arteriovenous fistula with marked ascending intramedullary venous drainage supplied by multiple feeding arteries from the radiculomeningeal arteries. The MIP axial image (F) reconstructed from the 3D-RA of the left vertebral artery shows the arteriovenous fistula presumed to be located in the left C5 intervertebral foramen. 3D-RA/3D-MR fusion images (slab MIP axial image (G) and coronal image (H), slab MIP coronal image with scheme (I)) show a clear 3D relationship with differential contrast between the detailed angioarchitecture of the AVF and surrounding tissue structure. The dura mater of the spinal nerve root sleeve is clearly visualized by a black line in contrast to the spinal fluid in the subarachnoid space. The shunt point is distinctly located in the intradural C5 nerve root sleeve, suggesting the location of the RAVF at the spinal nerve root with intramedullary venous drainage. The asterisk indicates the shunt point. The yellow line indicates the dura mater of the spinal canal. 3D-MR, three-dimensional-heavily T2-weighted volumetric magnetic resonance; 3D-RA, three-dimensional-rotational angiography; A-P, anterior-posterior; Lat, lateral; MIP, maximum intensity projection; MRI, magnetic resonance imaging; RAVF, radicular arteriovenous fistula.

spinal fluid, ligaments, nerve roots, and dura mater of the spinal canal.[17–20] Owing to high spatial resolution and isotropic data acquisition, multiplanar reconstruction in any plane is feasible by applying detailed evaluation of the SAVSs and allowing favorable registration during image fusion with other modalities.[18–20 22] Therefore, fusion images combined with the features of 3D-RA, which can reveal the fine angioarchitecture and the bony structures, and 3D-MRI, which can clearly reveal the surrounding anatomical landmarks, is expected to increase the understanding of SAVSs. During the creation of the fusion images, the target vessels of interest can be color coded according to user preference. Adjusting the threshold and thickness of the reconstructed images can be performed at the workstation, which would lead to a better understanding of the 3D anatomy. In our present results, the interobserver agreement for 3D-RA alone was not sufficient, especially for SDAVF, SEDAVF, and RAVF. This may be because the relationship between the dura mater and shunt point cannot be well delineated with 3D-RA alone. In fact, the dura mater was clearly distinguishable from the arachnoid space on 3D-MRI, which improved the diagnostic interobserver agreement using the 3D-RA/3D-MR fusion images. Moreover, from the fusion images, it is possible to speculate on the association between risky structures for vascular malformation, aneurysms, varices and any accompanying complications of SAVSs such as hematoma or spinal cord focal localized edema.

The treatment strategy to obtain complete obliteration of SAVSs is based on their angioarchitecture. Treatment outcomes differed among the types of SAVS.[2] The differences in angioarchitecture of spinal cord AVSs affect the complexity of treatment. Therefore, precise differentiation and identification

of their angioarchitecture is essential for the selection of an optimal treatment strategy.[3 5] The diagnostic significance of the shunt lesion is that clinical characteristics and outcomes differ depending on the type of SAVS. In SAVSs at the craniocervical junction, hemorrhagic presentation is significantly more frequent in RAVF, in which radical treatment is needed.[2] However, it is difficult to distinguish between RAVF with a shunt on the intradural spinal nerve root and SDAVF with a shunt on the dura mater of the spinal nerve root sleeve based on 3D-RA with conventional DSA because visualization of the true dura mater, spinal nerves, and subarachnoid space is not possible with 3D-RA. Furthermore, other clinical differences have been reported; the preoperative neurological deficits of SEDAVFs are more severe than those of SDAVFs, the rate of gradual onset of PMAVFs was significantly higher than that of SAVMs, and the natural history of symptomatic spinal cord AVSs is poor.[23 24] Therefore, there is a need to clearly delineate the shunt point of SAVSs. Multimodal fusion images are promising for the evaluation and understanding of their angioarchitecture along with the surrounding anatomy,[2 4 9 14 21] leading to the establishment of treatment strategies for both endovascular and surgical treatments.[10–12] Thus, we recommend using this fusion technique for obtaining the optimal diagnosis of SAVS in the clinical setting. In addition, proper diagnosis using fusion images would allow for the prediction of clinical outcomes and proper case management. These fusion images could alter the management and treatment strategy for SAVS, leading to better treatment results.

The present study has some limitations. This was a retrospective study with a relatively small sample size, given the rarity of the disease, and potentially involved selection biases. Therefore,
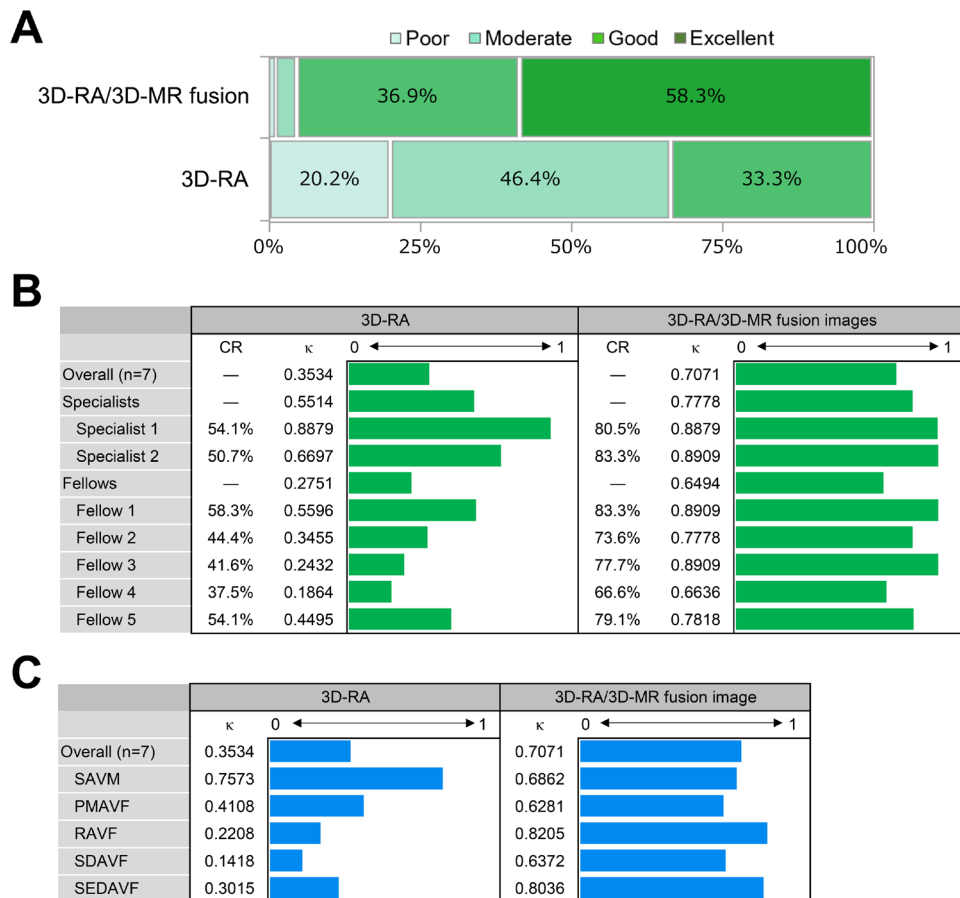
Figure 4 Interobserver agreement for the final diagnosis of SAVSs. (A) Assessment of image quality to delineate the relationship between the vessels and surrounding anatomical structures: 4-grade scale (excellent, good, moderate, poor). The image quality grade was significantly higher in the 3D-RA/3D-MR fusion image than in the 3D-RA image. (B) Interobserver agreements of the seven blinded reviewers for the SAVS diagnosis. Comparison of the kappa coefficient between the 3D-RA and 3D-RA/3D-MR fusion images. (C) Interobserver agreements for each diagnostic category. Comparison of the kappa coefficient between the 3D-RA and 3D-RA/3D-MR fusion images. 3D-MR, three-dimensional-heavily T2-weighted volumetric magnetic resonance; 3D-RA, three-dimensional-rotational angiography; CR, concordance rate; PMAVF, perimedullary arteriovenous fistula; RAVF, radicular arteriovenous fistula; SAVM, spinal arteriovenous malformation; SAVS, spinal arteriovenous shunts; SDAVF, spinal dural arteriovenous fistula; SEDAVF, spinal epidural arteriovenous fistula; κ, kappa coefficient.

generalization of the conclusions of this study may be limited. There were also some methodological limitations. First, unlike conventional DSA, 3D-RA/3D-MR fusion images do not provide temporal information on blood flow. This disadvantage may be eliminated with the use of a 4D-DSA dataset, instead of 3D-RA, for the fusion images.[13] Second, fusion of the different modality images may not be precisely obtained because the bony landmarks may change based on patient posture, breathing, and motion during the examination.[14] Diminution of the cerebrospinal fluid space in spinal canal stenosis or other pathologies could also hamper the identification of a fistula.[18] Therefore, fusion techniques require manual data corrections by well-experienced radiological technologists and neurointerventionalists. The possibility of misregistration should be considered as a detriment of fusion imaging.

CONCLUSION

We report the diagnostic accuracy of 3D-RA/3D-MR fusion images for the evaluation of SAVSs. 3D-RA/3D-MR fusion images provide high spatial resolution, allowing highly accurate and detailed evaluation of the anatomical structure surrounding the shunt. This fusion technique is promising for the evaluation of SAVS pathogenesis. It is expected to improve the overall diagnostic accuracy for SAVSs.

the article and its Supplementary Information, and can be obtained from the corresponding author on reasonable request.

Supplemental material This content has been supplied by the author(s). It has not been vetted by BMJ Publishing Group Limited (BMJ) and may not have been peer-reviewed. Any opinions or recommendations discussed are solely those of the author(s) and are not endorsed by BMJ. BMJ disclaims all liability and responsibility arising from any reliance placed on the content. Where the content includes any translated material, BMJ does not warrant the accuracy and reliability of the translations (including but not limited to local regulations, clinical guidelines, terminology, drug names and drug dosages), and is not responsible for any error and/or omissions arising from translation and adaptation or otherwise.

Open access This is an open access article distributed in accordance with the Creative Commons Attribution Non Commercial (CC BY-NC 4.0) license, which permits others to distribute, remix, adapt, build upon this work non-commercially, and license their derivative works on different terms, provided the original work is properly cited, appropriate credit is given, any changes made indicated, and the use is non-commercial. See: http://creativecommons.org/licenses/by-nc/4.0/.

ORCID iDs
Bikei Ryu http://orcid.org/0000-0003-0323-6628
Shinsuke Sato http://orcid.org/0000-0003-2911-6755

REFERENCES

1 Rodesch G, Lasjaunias P. Spinal cord arteriovenous shunts: from imaging to management. *Eur J Radiol* 2003;46:221–32.

2 Hiramatsu M, Sugiu K, Ishiguro T, *et al*. Angioarchitecture of arteriovenous fistulas at the craniocervical junction: a multicenter cohort study of 54 patients. *J Neurosurg* 2018;128:1839–49.

3 Hiu T, Kitagawa N, Morikawa M, *et al*. Efficacy of DynaCT digital angiography in the detection of the fistulous point of dural arteriovenous fistulas. *AJNR Am J Neuroradiol* 2009;30:487–91.

4 Ryu B, Sato S, Mochizuki T, *et al*. Spinal arteriovenous fistula located in the filum terminale externa: a case report and review of the literature. *Interv Neuroradiol* 2020:159101992096836.

5 Kiyosue H, Matsumaru Y, Niimi Y, *et al*. Angiographic and clinical characteristics of thoracolumbar spinal epidural and dural arteriovenous fistulas. *Stroke* 2017;48:3215–22.

6 Kiyosue H, Tanoue S, Okahara M, *et al*. Spinal ventral epidural arteriovenous fistulas of the lumbar spine: angioarchitecture and endovascular treatment. *Neuroradiology* 2013;55:327–36.

7 Prestigiacomo CJ, Niimi Y, Setton A, *et al*. Three-dimensional rotational spinal angiography in the evaluation and treatment of vascular malformations. *AJNR Am J Neuroradiol* 2003;24:1429–35.

8 Li Z-F, Hong B, Xv Y, *et al*. Using DynaCT rotational angiography for angioarchitecture evaluation and complication detection in spinal vascular diseases. *Clin Neurol Neurosurg* 2015;128:56–9.

9 Tanoue S, Endo H, Hiramatsu M, *et al*. Delineability and anatomical variations of perforating arteries from normal vertebral artery on 3D DSA: implications for endovascular treatment of dissecting aneurysms. *Neuroradiology* 2020. doi:10.1007/s00234-020-02549-y. [Epub ahead of print: 21 Sep 2020].

10 Shimizu S, Suzuki H, Maki H, *et al*. A novel image fusion visualizes the angioarchitecture of the perforating arteries in the brain. *AJNR Am J Neuroradiol* 2003;24:2011–4.

11 Sato M, Tateishi K, Murata H, *et al*. Three-dimensional multimodality fusion imaging as an educational and planning tool for deep-seated meningiomas. *Br J Neurosurg* 2018;32:509–15.

12 Ide S, Hirai T, Morioka M, *et al*. Usefulness of 3D DSA-MR fusion imaging in the pretreatment evaluation of brain arteriovenous malformations. *Acad Radiol* 2012;19:1345–52.

13 Tritt S, Ommer B, Gehrisch S, *et al*. Optimization of the surgical approach in AVMs using MRI and 4D DSA fusion technique: a technical note. *Clin Neuroradiol* 2017;27:443–50.

14 Takai K, Kin T, Oyama H, *et al*. The use of 3D computer graphics in the diagnosis and treatment of spinal vascular malformations. *J Neurosurg Spine* 2011;15:654–9.

15 Mandalapu S, Kannath S, Kesavadas C. Fusion imaging of time resolved imaging of contrast kinetics (TRICKS) and high resolution volumetric T2 MR sequences in the evaluation of spinal vascular malformations. *J Neuroradiol* 2019;46:276–7.

16 Crewson PE. Reader agreement studies. *AJR Am J Roentgenol* 2005;184:1391–7.

17 Baumert B, Wörtler K, Steffinger D, *et al*. Assessment of the internal craniocervical ligaments with a new magnetic resonance imaging sequence: three-dimensional turbo spin echo with variable flip-angle distribution (SPACE). *Magn Reson Imaging* 2009;27:954–60.

18 Kannath SK, Alampath P, Enakshy Rajan J, *et al*. Utility of 3D space T2-weighted volumetric sequence in the localization of spinal dural arteriovenous fistula. *J Neurosurg Spine* 2016;25:125–32.

19 Kannath SK, Mandapalu S, Thomas B, *et al*. Comparative analysis of volumetric high-resolution heavily T2-weighted MRI and time-resolved contrast-enhanced MRA in the evaluation of spinal vascular malformations. *AJNR Am J Neuroradiol* 2019;40:1601–6.

20 Kannath SK, Rajendran A, Thomas B, *et al*. Volumetric T2-weighted MRI improves the diagnostic accuracy of spinal vascular malformations: comparative analysis with a conventional MR study. *J Neurointerv Surg* 2019;11:1019–23.

21 Krings T, Lasjaunias PL, Hans FJ, *et al*. Imaging in spinal vascular disease. *Neuroimaging Clin N Am* 2007;17:57–72.

22 Morris JM, Kaufmann TJ, Campeau NG, *et al*. Volumetric myelographic magnetic resonance imaging to localize difficult-to-find spinal dural arteriovenous fistulas. *J Neurosurg Spine* 2011;14:398–404.

23 Yu J-X, Hong T, Krings T, *et al*. Natural history of spinal cord arteriovenous shunts: an observational study. *Brain* 2019;142:2265–75.

24 Takai K, Endo T, Yasuhara T, *et al*. Microsurgical versus endovascular treatment of spinal epidural arteriovenous fistulas with intradural venous drainage: a multicenter study of 81 patients. *J Neurosurg Spine* 2020:1–11.